## Toward Task Generalization via Memory Augmentation in Meta-Reinforcement Learning

#### Kaixi Bao

Department of Mechanical and Process Engineering ETH Zurich, Switzerland kaibao@ethz.ch

## Andreas Krause

Chenhao Li

ETH AI Center

ETH Zurich, Switzerland

chenhli@ethz.ch

Department of Computer Science ETH Zurich, Switzerland krausea@ethz.ch

## Yarden As ETH AI Center ETH Zurich, Switzerland yardas@ethz.ch

# krausea@ethz.ch

#### **Marco Hutter**

Department of Mechanical and Process Engineering ETH Zurich, Switzerland mahutter@ethz.ch

Abstract: Agents trained via reinforcement learning (RL) often struggle to perform well on tasks that differ from those encountered during training. This limitation presents a challenge to the broader deployment of RL in diverse and dynamic task settings. In this work, we introduce memory augmentation, a memory-based RL approach to improve task generalization. Our approach leverages task-structured augmentations to simulate plausible out-of-distribution scenarios and incorporates memory mechanisms to enable context-aware policy adaptation. Trained on a predefined set of tasks, our policy demonstrates the ability to generalize to unseen tasks through memory augmentation without requiring additional interactions with the environment. Through extensive simulation experiments and real-world hardware evaluations on legged locomotion tasks, we demonstrate that our approach achieves zero-shot generalization to unseen tasks while maintaining robust in-distribution performance and high sample efficiency.

Keywords: Meta-Reinforcement Learning, Memory Augmentation

## 1 Introduction

Reinforcement learning (RL) has made significant strides in training agents to perform complex tasks [1, 2, 3, 4, 5], achieving high performance in controlled settings. However, RL agents often struggle when faced with tasks outside their training distribution—a limitation known as the out-of-distribution (OOD) generalization challenge. This limitation restricts the applicability of RL policies to a broader range of tasks beyond those encountered during training [6, 7].

A common way to address this challenge is to increase training diversity to better encompass potential test-time conditions. Domain randomization [8, 9, 10], for instance, achieves this by varying environment parameters, thereby exposing agents to a wider range of training scenarios. However, as the extent of randomization increases, this method often suffers from reduced sample efficiency [11]. Additionally, increased variations during training can result in over-conservative strategies, especially in environments where these variations are not fully observable. In such settings, the agent may struggle to discern the current task parameterizations and only executes conservative moves, thereby sacrificing optimality. This raises a crucial question: how can an RL agent achieve robust

performance across diverse environment variations, or *tasks*, without being explicitly exposed to them during training?

A promising method to achieve this is through experience augmentation [12], where training experiences are augmented to simulate a broader range of potential test-time conditions. However, pure augmentation, without properly accounting for task context, may similarly cause overconservativeness resulting from exposing the policy to excessive unobservable variations. Building on the contextual modeling capability of Recurrent Neural Networks (RNNs), which have been shown to effectively address partial observability [13], we enhance experience augmentation in RL by incorporating memory mechanisms that respect the necessary task context.

In this work, we introduce *memory augmentation*, a novel approach to improve task generalization by augmenting training experience to simulate plausible OOD tasks and incorporating memory mechanisms to facilitate zero-shot task adaptation. Our approach trains a single unified policy that can perform well across both in-distribution (ID) and unseen OOD tasks.

In summary, our contributions include:

- We propose *memory augmentation*, a novel approach to improve task generalization without additional interactions with the environment.
- We validate our approach across a variety of legged locomotion experiments. Results demonstrate that our memory-augmented policies generalize effectively to unseen OOD tasks while maintaining robust ID performance. Additionally, while maintaining comparable performance, they achieve superior sample efficiency compared to randomization-based policies, where the agent is explicitly trained across all conditions.
- We demonstrate the sim-to-real transfer of the learned memory-augmented policy on a quadrupedal robot for position tracking under joint failure. The robot successfully tracks the goals while effectively adapting to both ID and OOD joint failures.

Supplementary videos for this work are available at https://sites.google.com/view/corl2025-ma/home.

## 2 Related Work

Task generalization remains a fundamental challenge in RL, as policies trained on a fixed set of tasks often fail to perform well under novel task conditions. A common strategy to address this challenge is domain randomization, originally introduced for sim-to-real transfer in robotics [8, 9, 10]. This approach randomizes environment parameters such as masses, friction coefficients, joint damping, and actuator gains during training to expose the agent to a wider range of conditions [10, 1, 2, 3, 14]. While it improves policy robustness, increased randomization often leads to reduced sample efficiency [11]. Alternatively, many works incorporate known physics principles or state structures into task design to approach task generalization. Examples include foot-placement dynamics [15], object invariance [16], granular media interactions [17], frequency domain parameterization [7], rigid body dynamics [18], and semi-structured Lagrangian dynamics models [19].

Some prior works have explored experience augmentation in RL, where original state-action trajectories are modified to enrich the training signal. For example, PlayVirtual [20] augments virtual trajectories using forward and backward dynamics in a latent space to enhance representation learning. Hindsight Experience Replay (HER) [12, 21, 22, 23, 24] relabels failed trajectories with alternative goals to provide more informative learning signals. In the context of legged locomotion, symmetry-based augmentation has been applied to encourage symmetry-invariant behavior [25, 26]. While these methods leverage experience augmentation to improve policy learning, they do not explicitly tackle the challenge of task generalization.

Another relevant line of research is meta-RL [27, 28, 29, 30], which enables agents to quickly adapt to new tasks by leveraging shared structure across tasks encountered during meta-training.

Memory-based meta-learners [29, 30], which encode task context through interaction history, have been leveraged for applications such as learning dynamics model priors for online adaptation [31] and training morphology-agnostic locomotion policies [32]. In LDM [33] and VariBAD Dream [34], experience augmentation is integrated into meta-RL by generating imagined tasks from the learned latent task space of a VariBAD [28] model to improve generalization. However, most meta-RL methods [27, 28, 29, 30, 34] focus on ID generalization, assuming test tasks are sampled from the same distribution as training tasks, and are not inherently equipped to handle OOD generalization. While LDM takes a step toward addressing this gap by generating imagined tasks through interpolation in the latent task space for OOD generalization, the resulting tasks may not accurately capture meaningful task structures, limiting generalization in complex environments. In this work, we contribute to addressing this challenge by integrating task-structured experience augmentation with memory-based meta-RL, enabling generalization to plausible OOD tasks.

#### 3 Preliminaries

#### 3.1 Partially observable Markov Decision Process and Meta-RL

We model the problem as a Partially Observable Markov Decision Process (POMDP). We define a POMDP as the tuple  $\mathcal{M}=\langle\mathcal{S},\mathcal{O},\mathcal{A},p,r,\gamma,\rho_0\rangle$ , where  $\mathcal{S}$  is the set of states,  $\mathcal{O}$  is the set of observations,  $\mathcal{A}$  is the set of actions,  $p:\mathcal{S}\times\mathcal{A}\times\mathcal{S}\to\mathbb{R}_{\geq 0}$  is the state transition function,  $r:\mathcal{S}\times\mathcal{A}\to\mathbb{R}$  is the reward function,  $\gamma$  is the discount factor, and  $\rho_0:\mathcal{S}\to\mathbb{R}_{\geq 0}$  is the initial state distribution. In POMDPs, observations provide only partial information about the true underlying state, requiring the agent to infer the latent state. In our setup, this latent state corresponds to the unobservable task context, such as an unknown payload on the robot's body, which remains fixed throughout each rollout. In conventional RL, the agent aims to learn a policy  $\pi$  that maximizes the expected cumulative reward:

$$J(\pi) = \mathbb{E}_{\tau \sim p_{\pi}(\tau)} \left[ \sum_{t=0}^{\infty} \gamma^{t} r(s_{t}, a_{t}) \right],$$

where  $\tau = (s_0, a_0, s_1, \dots)$  represents a trajectory sampled from the POMDP  $\mathcal{M}$  under policy  $\pi$ .

In this work, we frame the problem of learning across multiple tasks as a meta-RL problem, with the objective of optimizing over a distribution of tasks  $p(\mathcal{T})$ . In our setting, this corresponds to a distribution of POMDPs  $\mathcal{M}(\mathcal{T})$ . The goal is to learn a policy  $\pi$  that maximizes the expected cumulative reward across tasks:

$$J(\pi) = \mathbb{E}_{T \sim p(\mathcal{T}), \tau \sim p_{\pi}(\tau|T)} \left[ \sum_{t=0}^{\infty} \gamma^{t} r(s_{t}, a_{t}) \right].$$

#### 3.2 Problem statement

We consider a set of tasks  $\mathcal{T}$ , where  $\mathcal{T}_{ID} \subset \mathcal{T}$  represents the subset of tasks accessible during training, referred to as ID tasks. The remaining tasks,  $\mathcal{T}_{OOD} = \mathcal{T} \setminus \mathcal{T}_{ID}$ , constitute the set of unseen tasks that differ from the training tasks. In this work, we focus on a subset of these unseen tasks,  $\mathcal{T}_{OOD}^{aug} \subset \mathcal{T}_{OOD}$ , which can be effectively simulated through task-structured augmentations without requiring additional interactions with the environment. These tasks exhibit different dynamics from  $\mathcal{T}_{ID}$  while maintaining the same reward structure. Our goal is to train a single policy that can adapt and perform well across both  $\mathcal{T}_{ID}$  and  $\mathcal{T}_{OOD}^{aug}$ . This is formalized by maximizing the expected cumulative reward:

$$J(\pi) = \mathbb{E}_{T \sim p(\mathcal{T}_{\text{ID}} \cup \mathcal{T}_{\text{OOD}}^{\text{aug}}), \tau \sim p_{\pi}(\tau|T)} \left[ \sum_{t=0}^{\infty} \gamma^{t} r_{T}(s_{t}, a_{t}) \right].$$

During training, only partial observations are available for  $\mathcal{T}_{ID}$ . In this setting, the agent must infer the latent task context implicitly based on past observations and actions.

## 4 Approach

#### 4.1 Task-structured augmentation

To augment the training experience, our approach uses a set of transformation functions, denoted by  $\mathcal{G}$ , where each  $g \in \mathcal{G}$  represents a transformation reflecting the underlying structure assumed to exist in the task space. Formally, let  $\tau = \{(o_t, a_t, o_{t+1}, r_t)\}_{t=0}^T$  represent a trajectory collected by the current policy  $\pi_{\theta_k}$  within the training set  $\mathcal{T}_{\text{ID}}$ . Each transformation  $g = (g_o, g_a) \in \mathcal{G}$  consists of functions  $g_o : \mathcal{O} \to \mathcal{O}$  and  $g_a : \mathcal{A} \to \mathcal{A}$ , which map an observation-action pair (o, a) to a new pair  $(o^g, a^g) = (g_o(o), g_a(a))$ . Although transformations are applied at the observation level, we assume they are induced by consistent transformations at the underlying state level. For all  $g \in \mathcal{G}$ ,  $s \in \mathcal{S}$ ,  $a \in \mathcal{A}$ , it is assumed that the following properties hold:

- (a) **Transition probability invariance:** The effect of actions on state transitions remains unchanged under transformation, i.e.,  $p(s_{t+1}^g \mid s_t^g, a_t^g) = p(s_{t+1} \mid s_t, a_t)$ .
- (b) **Initial state distribution invariance:** Augmented episodes start from statistically equivalent conditions, i.e.,  $\rho_0(s^g) = \rho_0(s)$ .
- (c) **Reward invariance:** Transformed and original state-action pairs receive the same rewards in their respective tasks, i.e.,  $r(s_t^g, a_t^g) = r(s_t, a_t)$ .

These properties ensure that the transformed trajectories are behaviorally equivalent to the original ones in their respective tasks, allowing us to reuse the advantage estimates and action probabilities from the original rollouts during policy updates (see Sec. 4.2). The resulting transformed trajectory  $\tau_g = \{(o_t^g, a_t^g, o_{t+1}^g, r_t)\}_{t=0}^T \text{ represents the agent's simulated experience within an augmented task } T \in \mathcal{T}_{\text{OOD}}^{\text{oug}}, \text{ generated without real environment interactions.}$ 

An example of such transformations in  $\mathcal{G}$  includes symmetry transformations, which have been used in RL [35] for manipulation tasks [22] and legged locomotion control [25, 26]. Specifically, for quadrupedal robots, symmetry transformations can simulate mirrored conditions (e.g., joint failures) across left-right and front-back body parts. Similarly, for humanoid robots, they can replicate mirrored conditions across left-right body parts. These transformations leverage the morphological symmetry inherent to legged robots and uphold the essential invariance properties (a)–(c) [36].

### 4.2 Training with augmented data

We use Proximal Policy Optimization (PPO) [37] as the underlying RL algorithm. Following the method of Mittal et al. [25], we approach data augmentation in PPO by constructing augmented policies  $\pi^g_{\theta_k}$  such that  $\pi^g_{\theta_k}(a^g|s^g) = \pi_{\theta_k}(a|s), \forall g \in \mathcal{G}, s \in \mathcal{S}, a \in \mathcal{A}$ . Based on properties (a)–(c), it can be shown that the advantage function and state probability distribution are preserved under transformation, i.e.,  $A^{\pi^g_{\theta_k}}(s^g, a^g) = A^{\pi_{\theta_k}}(s, a)$ , and  $p_{\pi^g_{\theta_k}}(s^g) = p_{\pi_{\theta_k}}(s)$  [25]. These invariances allow the policy update to incorporate augmented trajectories while retaining the action probabilities of the original data. For further details, we refer readers to [25].

For each gradient update, we sample a mini-batch of trajectories from the original rollouts along with their corresponding transformed trajectories:

$$\mathcal{D}_{\text{minibatch}} = \{\tau_i\}_{i=1}^{N_{\text{minibatch}}} \cup \bigcup_{g \in \mathcal{G}} \{\tau_i^g\}_{i=1}^{N_{\text{minibatch}}}.$$

This approach ensures balanced learning across both the original and augmented tasks by maintaining equal representation for each task during the policy update.

#### 4.3 Memory augmentation

While experience augmentation can enhance generalization by increasing training diversity, the resulting variations, combined with the partially observable nature of the environment, may cause the

agent to adopt over-conservative strategies as it struggles to infer the latent task context. To address this limitation, we extend augmentation to the agent's memory by incorporating an RNN into the training framework, as illustrated in Fig. 1. The RNN, leveraging its context modeling capability, acts as an implicit task encoder. At each time step, the RNN updates its hidden state  $h_t$  based on the observations, progressively capturing task-specific information accumulated so far. From this hidden state, the RNN generates a latent task embedding  $z_t$ , which conditions the policy, allowing it to adapt decisions based on the inferred context.

In addition to augmenting trajectories, we extend the RNN's hidden states to incorporate memory for the augmented tasks. As shown in Fig. 2, this is achieved by performing a forward pass with the transformed observation sequence  $(o_t^g)_{t=0}^T$  through the RNN. During this process, the RNN generates a sequence of hidden states  $(h_t^g)_{t=0}^T$  that progressively encode the evolving dynamics of the augmented observations. To ensure continuity in the context encoding, the initial hidden state  $h_0^{g,k}$  for the current update k is set to the final hidden state

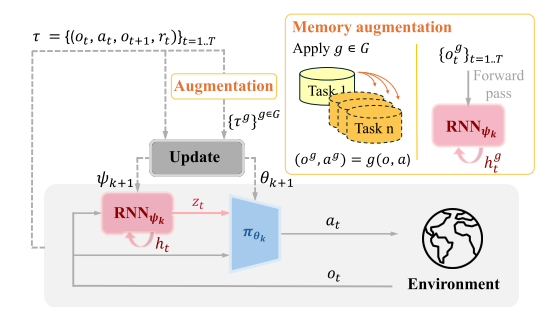


Figure 1: Overview of our training framework.

 $h_T^{g,k-1}$  from the previous update. The forward pass is performed continuously throughout the episode to ensure that the RNN's hidden states capture the cumulative dynamics of the augmented observations at each step, providing an up-to-date context encoding for subsequent updates. The resulting latent task embeddings  $(z_t^g)_{t=0}^T$  provide the policy with the inferred context of the augmented tasks. This memory augmentation allows the policy to infer unobservable context information for both ID and augmented scenarios. In contrast, a simple feedforward policy without memory cannot infer latent task context from partial observations, which may lead to degraded ID performance when augmented data is introduced.

## 5 Experiments

#### 5.1 Environment and task setup

We evaluate our approach across eight legged locomotion tasks using the ANYmal D quadruped and Unitree G1 humanoid robots in Isaac Lab [38]. The tasks are structured around position and velocity tracking, with variations introduced through simulated joint failures and diverse payload configura-

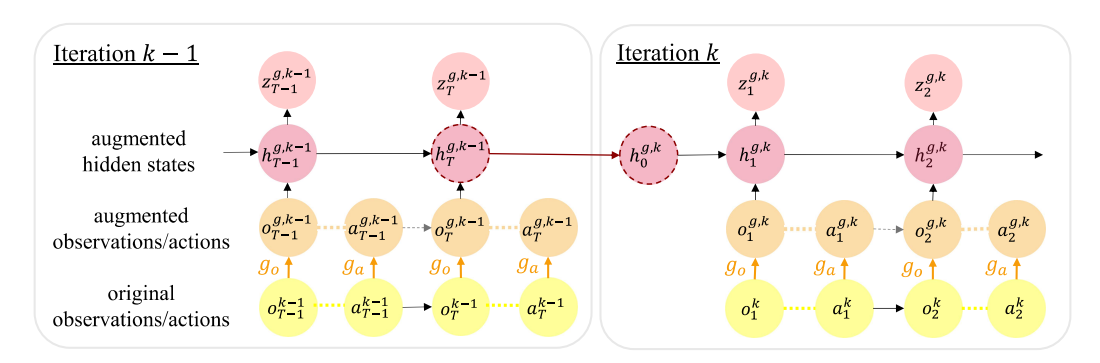
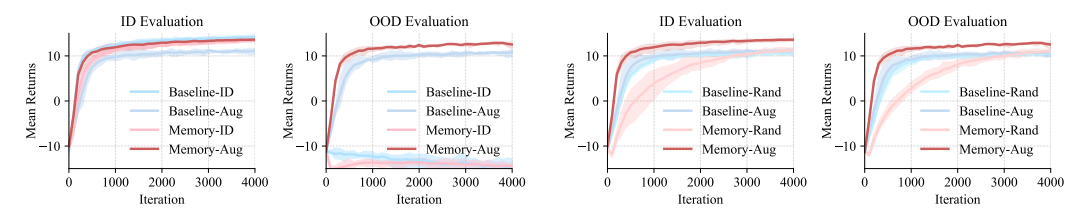


Figure 2: Memory augmentation. Transformation  $g=(g_o,g_a)\in\mathcal{G}$  is applied to observations  $o_t$  and actions  $a_t^g$  to generate augmented observations  $o_t^g$  and actions  $a_t^g$ . The augmented observation sequence is forward passed through the RNN, producing hidden states  $h_t^g$ . During the k-th policy update, the initial augmented hidden state  $h_0^{g,k}$  is set to the last hidden state from the previous update  $h_T^{g,k-1}$ , ensuring continuity and context retention across updates.



- (a) **Memory-Aug** avoids the ID performance degradation observed in **Baseline-Aug**.
- (b) **Memory-Aug** achieves performance comparable to **Memory-Rand** with higher sample efficiency.

Figure 3: Evaluation of quadruped position tracking under joint failure.

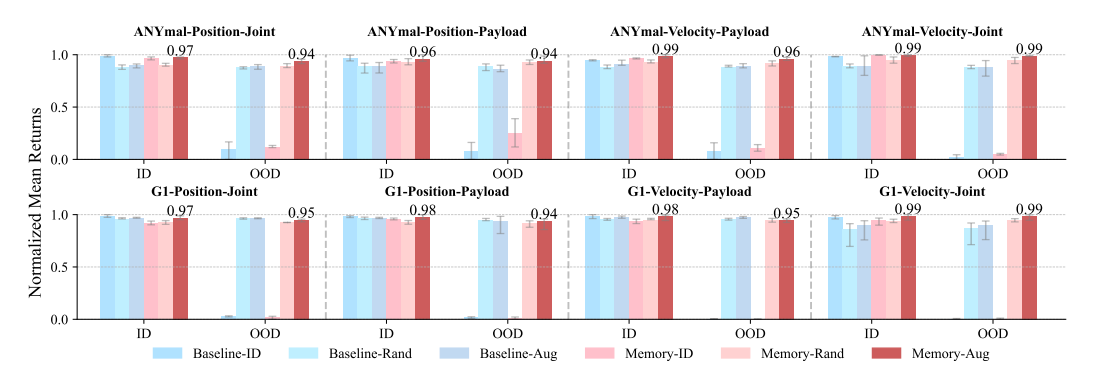


Figure 4: Normalized mean episodic returns on ID and OOD tasks. **Memory-Aug** generalizes well to OOD tasks while preserving strong ID performance across all experiments.

tions to test both ID and OOD task generalization. We compare policies trained with (**-Aug**) and without (**-ID**) experience augmentation, using both memory-based (**Memory-**) and standard MLP (**Baseline-**) architectures. Additional baselines include randomized training over all task conditions (**-Rand**). Full task setup and training details are provided in the Appendix.

#### 5.2 Task performance and data efficiency

Figure 3 presents ID and OOD evaluations of different policies in quadruped position tracking under joint failure scenarios. As shown in Fig. 3b, **Baseline-Aug** exhibits ID performance comparable to **Baseline-Rand**, but falls short of matching the ID performance of **Baseline-ID** (see Fig. 3a). These findings highlight how variations introduced through randomization or augmentation can cause a simple MLP policy to adopt suboptimal behaviors in partially observable settings. Lacking the ability to infer latent task context from partial observations, such policies resort to over-conservative strategies, limiting their ability to optimize performance in specific tasks. In contrast, **Memory-Aug** achieves performance comparable to **Memory-ID** on ID tasks. This result demonstrates that the memory module effectively captures task context from partial observations and leverages it in experience augmentation, thereby preserving robust ID performance. Furthermore, **Memory-Aug** attains performance on par with **Memory-Rand** in both ID and OOD tasks. Notably, **Memory-Aug** achieves this without requiring any additional environment interactions for these OOD tasks, demonstrating higher sample efficiency than **Memory-Rand**.

Next, we evaluate our approach across different robot embodiments (quadruped and humanoid), task types (position and velocity tracking), and variations in task conditions (joint failures and payload distributions). As shown in Fig. 4, the ID performance degradation in **Baseline-Rand** and **Baseline-Aug** persists, particularly in quadruped experiments, where task diversity is more pronounced. In contrast, **Memory-Rand** and **Memory-Aug** consistently match the ID performance of **Memory-ID**. By inferring latent task context from past experience, the memory module enables robust ID performance, even when trained under diverse task conditions. Furthermore, **Memory-Aug** consistently

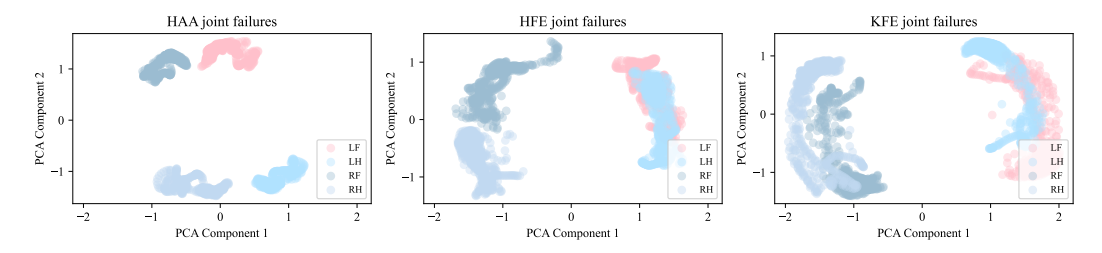


Figure 5: PCA visualization of latent task embeddings z (LF, in red) and  $z_g$  (RF, LH, RH, in blue) for joint failures across different joint types (HAA, HFE and KFE). The distinct clustering of tasks suggests that the learned latent space effectively captures task-specific features.

matches the performance of **Memory-Rand** in both ID and OOD tasks without requiring additional environment interactions, thereby improving sample efficiency.

#### 5.2.1 Latent task embedding analysis

To better understand how **Memory-Aug** policy captures task information, we analyze the latent task embeddings z and  $z_g$  produced by the memory module in the quadruped position tracking task under joint failures. Figure 5 presents a PCA visualization of the latent embeddings collected across various joint failure scenarios. Notably, the embeddings reveal an emergent symmetry across different legs. This spatial symmetry in the latent representation aligns closely with the physical symmetry of the robot's morphology and the underlying task structure. This finding highlights the capacity of the memory module to infer and encode unobservable task context, allowing the policy to adapt effectively to both ID and augmented task conditions.

#### 5.3 Behavior analysis with memory augmentation

We observe distinct foot movement patterns across policies in the quadruped position tracking task under joint failures. As shown in Fig. 6, **Baseline-Rand** and **Baseline-Aug** exhibit shorter air time and higher contact frequency compared to **Baseline-ID** under ID conditions. This indicates a cautious locomotion strategy characterized by smaller steps and frequent ground contact. The same pattern persists under OOD joint failures, indicating a lack of task-specific adaptation and a tendency toward

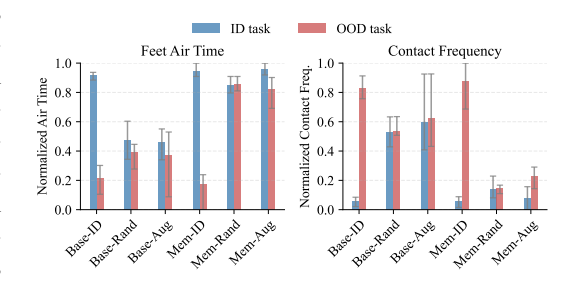


Figure 6: Motion analysis.

over-conservative movements. In contrast, **Memory-Rand** and **Memory-Aug** exhibit feet air time and contact frequency comparable to **Memory-ID** in ID tasks while maintaining similar levels in OOD tasks. We attribute this consistency to the memory module's ability to infer latent task context from partial observations, enabling context-aware adaptation.

In addition, we qualitatively examine how agents trained with different policies track goals. Figure 7 illustrates representative behaviors under an ID KFE joint failure. As shown on the left, agents trained with **Baseline-Rand** and **Baseline-Aug** tend to walk directly toward the goal using small, cautious steps. This conservative behavior aligns with the quantitative findings in Fig. 6, where these policies exhibited shorter foot air time and higher contact frequency. The observed strategy suggests a uniform reduction in joint usage rather than targeted compensation for the impaired joint. As a result, these agents often stumble or passively drift in orientation. In contrast, agents trained with **Baseline-ID** and **Memory-ID** adopt more adaptive behaviors. They first reorient their bodies sideways toward the goal, then move laterally while dragging the impaired leg to reduce reliance on the failed joint (see upper row of Fig. 7). This intentional body adjustment supports more stable and effective goal tracking. Notably, **Memory-Rand** and **Memory-Aug** agents demonstrate similarly

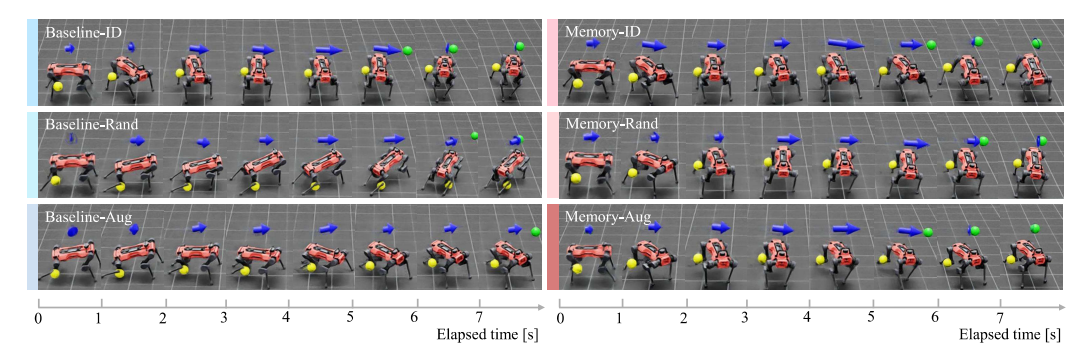


Figure 7: Behavior analysis of different policies for quadruped position tracking under an ID KFE joint failure (yellow marker). The blue arrow indicates base velocity; the green marker shows the goal. *Left:* The **Baseline-ID** agent actively turns sideways toward the goal within the first second and moves laterally, dragging the impaired leg to reduce reliance on it. In contrast, **Baseline-Rand** and **Baseline-Aug** agents take small forward steps, often stumbling and passively drifting in orientation during tracking. *Right:* Memory-enabled agents actively adjust their body orientation within the first second, effectively compensating for the impaired joint and maintaining stable locomotion.

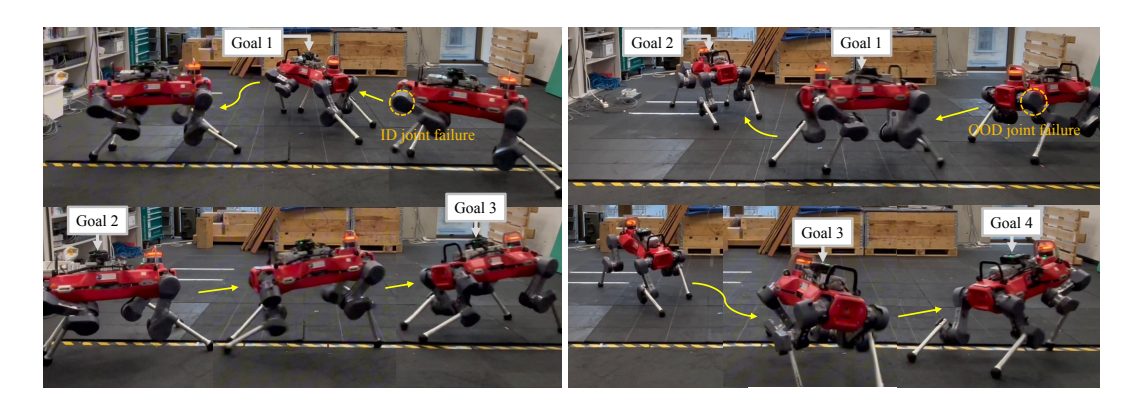


Figure 8: Hardware experiment. The **Memory-Aug**-trained agent successfully tracks goals under both ID (LF HAA) and OOD (RH HAA) joint failures.

adaptive behaviors, highlighting the memory module's ability to infer latent task context, including the presence and nature of joint failures, and enable targeted adaptation.

#### 5.4 Hardware experiments

We deploy our **Memory-Aug** policy on the ANYmal D robot for position tracking under joint failure. To facilitate sim-to-real transfer, we introduce randomization in terrain profiles with a noise range of [0.0, 0.05] during training. As shown in Fig. 8, the robot successfully tracks multiple goals while adapting to both ID and OOD joint failures. These results demonstrate the ID robustness and OOD generalization capability of the memory-augmented policy in real-world deployment.

## 6 Conclusion

In this work, we present *memory augmentation*, an RL framework that integrates task-structured experience augmentation with memory mechanisms to enhance task generalization. By simulating varied task conditions through augmented training experiences and incorporating memory-based task inference, our approach trains a single unified policy capable of handling both ID and OOD tasks without additional environment interactions. Our approach addresses the limitations of context-unaware policies, which tend to adopt over-conservative strategies in highly randomized and par-

tially observable environments. Extensive simulation results show that our method achieves zero-shot generalization to OOD tasks while maintaining strong ID performance. Furthermore, our approach demonstrates performance comparable to domain randomization in both ID and OOD tasks without incurring the additional sample cost typically required to expose the agent to OOD conditions during training. Crucially, the memory mechanism proves essential in supporting reliable adaptation across diverse tasks under partial observabilities. Finally, hardware experiments on a quadruped robot demonstrate the effectiveness of our approach in real-world settings, validating sim-to-real transfer for both ID and OOD scenarios. We believe this work inspires further advancements in developing adaptive RL agents capable of handling the complexities and uncertainties of real-world environments.

#### Limitations

Our work relies on prior knowledge of the task structure to augment the training experience and simulate diverse task conditions. A key limitation, however, lies in the restricted set of transformations that satisfy the required invariance assumptions to ensure the safe incorporation of augmented data into the policy update. This constraint narrows the range of task variations we can simulate, limiting generalization in scenarios where suitable transformations are difficult to define or do not preserve the required properties. That said, this reliance also allows for the principled design of augmentations that are grounded in domain-specific insights and aligned with the inherent structure of the task. More flexible techniques for experience augmentation would enable simulation of a wider range of OOD task conditions and enhance generalization across diverse and unstructured environments. While this paper demonstrates the utility of experience augmentation for task generalization under simple symmetry transformations, extending its applicability to more flexible augmentation techniques is left for future work.

#### References

- [1] J. Lee, J. Hwangbo, L. Wellhausen, V. Koltun, and M. Hutter. Learning quadrupedal locomotion over challenging terrain. *Science robotics*, 5(47):eabc5986, 2020. URL https://www.science.org/doi/epdf/10.1126/scirobotics.abc5986.
- [2] A. Kumar, Z. Fu, D. Pathak, and J. Malik. Rma: Rapid motor adaptation for legged robots. *arXiv preprint arXiv:2107.04034*, 2021. URL https://arxiv.org/pdf/2107.04034.
- [3] T. Miki, J. Lee, J. Hwangbo, L. Wellhausen, V. Koltun, and M. Hutter. Learning robust perceptive locomotion for quadrupedal robots in the wild. *Science robotics*, 7(62):eabk2822, 2022. URL https://www.science.org/doi/abs/10.1126/scirobotics.abk2822.
- [4] D. Hoeller, N. Rudin, D. Sako, and M. Hutter. Anymal parkour: Learning agile navigation for quadrupedal robots. *Science Robotics*, 9(88):eadi7566, 2024. URL https://www.science.org/doi/epdf/10.1126/scirobotics.adi7566.
- [5] C. Li, M. Vlastelica, S. Blaes, J. Frey, F. Grimminger, and G. Martius. Learning agile skills via adversarial imitation of rough partial demonstrations. In *Conference on Robot Learning*, pages 342–352. PMLR, 2023. URL https://proceedings.mlr.press/v205/li23b.html.
- [6] C. Li, S. Blaes, P. Kolev, M. Vlastelica, J. Frey, and G. Martius. Versatile skill control via self-supervised adversarial imitation of unlabeled mixed motions. In 2023 IEEE international conference on robotics and automation (ICRA), pages 2944–2950. IEEE, 2023. URL https://ieeexplore.ieee.org/stamp/stamp.jsp?tp=&arnumber=10160421.
- [7] C. Li, E. Stanger-Jones, S. Heim, and S. Kim. Fld: Fourier latent dynamics for structured motion representation and learning. *arXiv preprint arXiv:2402.13820*, 2024. URL https://arxiv.org/pdf/2402.13820.
- [8] J. Tobin, R. Fong, A. Ray, J. Schneider, W. Zaremba, and P. Abbeel. Domain randomization for transferring deep neural networks from simulation to the real world. In 2017 IEEE/RSJ international conference on intelligent robots and systems (IROS), pages 23–30. IEEE, 2017. URL https://ieeexplore.ieee.org/stamp/stamp.jsp?tp=&arnumber=8202133.
- [9] F. Sadeghi and S. Levine. Cad2rl: Real single-image flight without a single real image. *arXiv* preprint arXiv:1611.04201, 2016. URL https://arxiv.org/pdf/1611.04201.
- [10] X. B. Peng, M. Andrychowicz, W. Zaremba, and P. Abbeel. Sim-to-real transfer of robotic control with dynamics randomization. In 2018 IEEE international conference on robotics and automation (ICRA), pages 3803–3810. IEEE, 2018. URL https://ieeexplore.ieee.org/stamp/stamp.jsp?tp=&arnumber=8460528.

- [11] R. Kirk, A. Zhang, E. Grefenstette, and T. Rocktäschel. A survey of zero-shot generalisation in deep reinforcement learning. *Journal of Artificial Intelligence Research*, 76:201–264, 2023. URL https://www.jair.org/index.php/jair/article/view/14174.
- [12] M. Andrychowicz, F. Wolski, A. Ray, J. Schneider, R. Fong, P. Welinder, B. McGrew, J. Tobin, O. Pieter Abbeel, and W. Zaremba. Hindsight experience replay. *Advances in neural information processing systems*, 30, 2017. URL https://proceedings.neurips.cc/paper/2017/hash/453fadbd8a1a3af50a9df4df899537b5-Abstract.html.
- [13] N. Heess, J. J. Hunt, T. P. Lillicrap, and D. Silver. Memory-based control with recurrent neural networks. *arXiv preprint arXiv:1512.04455*, 2015. URL https://arxiv.org/pdf/1512.04455.
- [14] O. M. Andrychowicz, B. Baker, M. Chociej, R. Jozefowicz, B. McGrew, J. Pachocki, A. Petron, M. Plappert, G. Powell, A. Ray, et al. Learning dexterous in-hand manipulation. *The International Journal of Robotics Research*, 39(1):3–20, 2020. URL https://journals.sagepub.com/doi/full/10.1177/0278364919887447.
- [15] Y. Yang, K. Caluwaerts, A. Iscen, T. Zhang, J. Tan, and V. Sindhwani. Data efficient reinforcement learning for legged robots. In *Conference on Robot Learning*, pages 1–10. PMLR, 2020. URL https://proceedings.mlr.press/v100/yang20a.html.
- [16] C. Sancaktar, S. Blaes, and G. Martius. Curious exploration via structured world models yields zero-shot object manipulation. *Advances in Neural Information Processing Systems*, 35: 24170–24183, 2022. URL https://proceedings.neurips.cc/paper\_files/paper/2022/hash/98ecdc722006c2959babbdbdeb22eb75-Abstract-Conference.html.
- [17] S. Choi, G. Ji, J. Park, H. Kim, J. Mun, J. H. Lee, and J. Hwangbo. Learning quadrupedal locomotion on deformable terrain. *Science Robotics*, 8(74):eade2256, 2023. URL https://www.science.org/doi/epdf/10.1126/scirobotics.ade2256.
- [18] Y. Song, S. Kim, and D. Scaramuzza. Learning quadruped locomotion using differentiable simulation. *arXiv preprint arXiv:2403.14864*, 2024. URL https://arxiv.org/pdf/2403.14864.
- [19] J. Levy, T. Westenbroek, and D. Fridovich-Keil. Learning to walk from three minutes of real-world data with semi-structured dynamics models. arXiv preprint arXiv:2410.09163, 2024. URL https://arxiv.org/pdf/2410.09163.
- [20] T. Yu, C. Lan, W. Zeng, M. Feng, Z. Zhang, and Z. Chen. Playvirtual: Augmenting cycle-consistent virtual trajectories for reinforcement learning. *Advances in Neural Information Processing Systems*, 34:5276–5289, 2021. URL https://proceedings.neurips.cc/paper/2021/hash/2a38a4a9316c49e5a833517c45d31070-Abstract.html.
- [21] M. Fang, T. Zhou, Y. Du, L. Han, and Z. Zhang. Curriculum-guided hind-sight experience replay. Advances in neural information processing systems, 32, 2019. URL https://proceedings.neurips.cc/paper/2019/hash/83715fd4755b33f9c3958e1a9ee221e1-Abstract.html.
- [22] Y. Lin, J. Huang, M. Zimmer, Y. Guan, J. Rojas, and P. Weng. Invariant transform experience replay: Data augmentation for deep reinforcement learning. *IEEE Robotics and Automation Letters*, 5(4):6615–6622, 2020. URL https://ieeexplore.ieee.org/stamp/stamp.jsp?tp=&arnumber=9158366.
- [23] R. Yang, M. Fang, L. Han, Y. Du, F. Luo, and X. Li. Mher: Model-based hindsight experience replay. *arXiv preprint arXiv:2107.00306*, 2021. URL https://arxiv.org/pdf/2107.00306.

- [24] C. Packer, P. Abbeel, and J. E. Gonzalez. Hindsight task relabelling: Experience replay for sparse reward meta-rl. Advances in neural information processing systems, 34:2466-2477, 2021. URL https://proceedings.neurips.cc/paper/2021/hash/1454ca2270599546dfcd2a3700e4d2f1-Abstract.html.
- [25] M. Mittal, N. Rudin, V. Klemm, A. Allshire, and M. Hutter. Symmetry considerations for learning task symmetric robot policies. 2024 IEEE International Conference on Robotics and Automation (ICRA), pages 7433–7439, 2024. URL https://arxiv.org/pdf/2403.04359.
- [26] Z. Su, X. Huang, D. Ordoñez-Apraez, Y. Li, Z. Li, Q. Liao, G. Turrisi, M. Pontil, C. Semini, Y. Wu, et al. Leveraging symmetry in rl-based legged locomotion control. *arXiv e-prints*, pages arXiv-2403, 2024. URL https://arxiv.org/pdf/2403.17320.
- [27] C. Finn, P. Abbeel, and S. Levine. Model-agnostic meta-learning for fast adaptation of deep networks. In *International conference on machine learning*, pages 1126–1135. PMLR, 2017. URL https://proceedings.mlr.press/v70/finn17a.html.
- [28] L. Zintgraf, K. Shiarlis, M. Igl, S. Schulze, Y. Gal, K. Hofmann, and S. Whiteson. Varibad: A very good method for bayes-adaptive deep rl via meta-learning. *arXiv* preprint *arXiv*:1910.08348, 2019. URL https://arxiv.org/pdf/1611.05763.
- [29] Y. Duan, J. Schulman, X. Chen, P. L. Bartlett, I. Sutskever, and P. Abbeel. RL<sup>2</sup>: Fast reinforcement learning via slow reinforcement learning. *arXiv preprint arXiv:1611.02779*, 2016. URL https://arxiv.org/pdf/1611.02779.
- [30] J. X. Wang, Z. Kurth-Nelson, D. Tirumala, H. Soyer, J. Z. Leibo, R. Munos, C. Blundell, D. Kumaran, and M. Botvinick. Learning to reinforcement learn. *arXiv preprint* arXiv:1611.05763, 2016. URL https://arxiv.org/pdf/1611.05763.
- [31] A. Nagabandi, I. Clavera, S. Liu, R. S. Fearing, P. Abbeel, S. Levine, and C. Finn. Learning to adapt in dynamic, real-world environments through meta-reinforcement learning. *arXiv* preprint arXiv:1803.11347, 2018. URL https://arxiv.org/pdf/1803.11347.
- [32] F. Zargarbashi, F. Di Giuro, J. Cheng, D. Kang, B. Sukhija, and S. Coros. Metaloco: Universal quadrupedal locomotion with meta-reinforcement learning and motion imitation. *arXiv* preprint arXiv:2407.17502, 2024. URL https://arxiv.org/pdf/2407.17502.
- [33] S. Lee and S.-Y. Chung. Improving generalization in meta-rl with imaginary tasks from latent dynamics mixture. *Advances in Neural Information Processing Systems*, 34:27222–27235, 2021.
- [34] Z. Rimon, A. Tamar, and G. Adler. Meta reinforcement learning with finite training tasks-a density estimation approach. *Advances in Neural Information Processing Systems*, 35: 13640–13653, 2022. URL https://proceedings.neurips.cc/paper\_files/paper/2022/hash/5833b4daf5b076dd1cdb362b163dff0c-Abstract-Conference.html.
- [35] R. De Santi, F. A. Joseph, N. Liniger, M. Mutti, and A. Krause. Geometric active exploration in markov decision processes: the benefit of abstraction. *arXiv* preprint arXiv:2407.13364, 2024.
- [36] D. Ordoñez-Apraez, G. Turrisi, V. Kostic, M. Martin, A. Agudo, F. Moreno-Noguer, M. Pontil, C. Semini, and C. Mastalli. Morphological symmetries in robotics. *arXiv* preprint *arXiv*:2402.15552, 2024. URL https://arxiv.org/pdf/2402.15552.
- [37] J. Schulman, F. Wolski, P. Dhariwal, A. Radford, and O. Klimov. Proximal policy optimization algorithms. *arXiv preprint arXiv:1707.06347*, 2017. URL https://arxiv.org/pdf/1707.06347.

- [38] M. Mittal, C. Yu, Q. Yu, J. Liu, N. Rudin, D. Hoeller, J. L. Yuan, R. Singh, Y. Guo, H. Mazhar, et al. Orbit: A unified simulation framework for interactive robot learning environments. *IEEE Robotics and Automation Letters*, 8(6):3740-3747, 2023. URL https://ieeexplore.ieee.org/stamp/stamp.jsp?tp=&arnumber=10107764.
- [39] N. Rudin, D. Hoeller, M. Bjelonic, and M. Hutter. Advanced skills by learning locomotion and local navigation end-to-end. In 2022 IEEE/RSJ International Conference on Intelligent Robots and Systems (IROS), pages 2497–2503. IEEE, 2022. URL https://ieeexplore.ieee.org/stamp/stamp.jsp?tp=&arnumber=9981198.

## A Appendix

#### A.1 Training algorithm

Algorithm 1 outlines our training process with memory augmentation.

### Algorithm 1 Recurrent PPO with Memory Augmentation

```
Input: Number of iterations N_{\text{iter}}
Output: Optimal policy and RNN parameters \theta^*, \psi^*
 1: Initialize environment, policy \pi_{\theta} and RNN<sub>\psi</sub>;
 2: Initialize hyperparameters \epsilon, \gamma;
 3: Define transformation set \mathcal{G} for experience augmentation;
 4: for k = 1, ..., N_{\text{iter}} do
 5:
           Collect rollouts \mathcal{D}_{\text{ID}} using \pi_{\theta};
           Generate \mathcal{D}_{\text{aug}}^{\text{OOD}} by applying transformations g \in \mathcal{G};
 6:
           Update RNN hidden states via forward pass;
 7:
           Combine rollouts: \mathcal{D}_{\text{train}} \leftarrow \mathcal{D}_{\text{ID}} \cup \mathcal{D}_{\text{aug}}^{\text{OOI}}
 8:
           for \mathcal{D}_{minibatch} sampled from \mathcal{D}_{train} do
 9:
                 Compute surrogate objective L_{\text{clip}};
10:
                 Update \theta and \psi;
11:
12:
           end for
13: end for
14: return \theta^*, \psi^*
```

#### A.2 Experiment details

#### A.2.1 Environment and task setup

Our experiments focus on two primary task settings:

- Position tracking: The robot's objective is to track a target position, sampled uniformly in polar coordinates with a radius between 1 m and 5 m around its initial position (i.e.,  $r \sim U([1.0, 5.0]), \ \theta \sim U([-\pi, \pi])$ ). The target position is dynamically converted to Cartesian coordinates  $\mathbf{x}_{b}^{\mathrm{cmd}} = [x_{b, \mathbf{x}}^{\mathrm{cmd}}, x_{b, \mathbf{y}}^{\mathrm{cmd}}] \in \mathbb{R}^2$ , relative to the robot's base frame based on its current position. This relative target position is provided as input to the policy, which outputs the target joint position  $\mathbf{q}^*$ . The episode length is set to  $8 \, \mathrm{s}$ .
- *Velocity tracking*: The robot's objective is to track a velocity command,  $\mathbf{v}^{\text{cmd}} = [v_x^{\text{cmd}}, v_y^{\text{cmd}}, \omega_z^{\text{cmd}}] \in \mathbb{R}^3$ , where  $v_{\text{cx}}^{\text{cmd}}$  and  $v_{\text{cy}}^{\text{cmd}}$  represent the target forward and lateral linear velocities, and  $\omega_z^{\text{cmd}}$  denotes the target yaw angular velocity. At the start of each episode, the velocity commands are sampled as follows:
  - Quadruped robot: The forward and lateral linear velocities are sampled uniformly between -1.0 and 1.0 m/s:

$$v_x^{\rm cmd} \sim U([-1.0, 1.0]), \quad v_y^{\rm cmd} \sim U([-1.0, 1.0]).$$

 Humanoid robot: The forward linear velocity is sampled uniformly between 0.0 and 1.0 m/s:

$$v_x^{\rm cmd} \sim U([0.0, 1.0]),$$

while the lateral velocity is fixed at zero:

$$v_y^{\rm cmd}=0.0.$$

A target heading direction is sampled uniformly from  $[-\pi, \pi]$ . The yaw command,  $\omega_z^{cmd}$ , is dynamically computed based on the target and current heading. The policy is trained to output the target joint position  $\mathbf{q}^*$ .

Additionally, we introduce variations to simulate joint failures and payload distributions:

- Joint failure: A joint failure is simulated by disabling the motor torque.
  - Quadruped robot: During training, a joint in the left front leg (LF HAA, LF HFE, or LF KFE) is randomly disabled, categorized as an ID joint failure. Joint failures in other legs are considered OOD failures.
  - **Humanoid robot:** A joint in the left hip (pitch, roll, or yaw) is randomly disabled during training (ID). Joint failures in the right hip are considered as OOD.

For both robots, a joint failure occurs with an 80% probability during training.

- Payload: A payload is simulated by imposing a vertical external force.
  - Quadruped robot: During training, a payload with a mass uniformly sampled from [30 kg, 40 kg] is applied at a random position on the left front section of the robot's base (ID). Payloads with the same mass range applied to other sections of the base are considered OOD.
  - Humanoid robot: During training, a payload with a mass uniformly sampled from [40 kg, 50 kg] is applied at a random position on the left shoulder of the robot (ID).
     Payloads applied to the right shoulder are considered OOD.

We train a memory-based policy both with and without experience augmentation, referred to as **Memory-Aug** and **Memory-ID**, respectively. To assess the role of memory-based task inference, we also train a standard MLP policy with experience augmentation [25, 26], referred to as **Baseline-Aug**, and a standard MLP policy without augmentation, referred to as **Baseline-ID**. Additionally, we include randomization-based policies, where the agent is exposed to all variations mentioned above (ID + OOD) during training. These are referred to as **Baseline-Rand** for the MLP-only architecture and **Memory-Rand** for the memory-enabled architecture. Training for each policy was conducted using five different seeds.

Tables S1–S6 summarize the observations, reward terms and training details for all task settings.

Term	Notation	Dimension ANYmal   G1	Units	Noise
Observations				
Base linear velocity	$\mathbf{v}_t$	3	m/s	[-0.10, 0.10]
Base angular velocity	$oldsymbol{\omega}_t$	3	rad/s	[-0.20, 0.20]
Projected gravity	$\mathbf{g}_t^{ ext{proj}}$	3	-	[-0.05, 0.05]
Joint position	$\mathbf{q}_t$	12   37	rad	[-0.01, 0.01]
Joint velocity	$\dot{f q}_t$	12   37	rad/s	[-1.50, 1.50]
Previous action	$\mathbf{a}_{t-1}$	12   37	rad	-
Normalized remaining time	$t_{ m left}$	1	-	-
Commands				
Target xy position	$\mathbf{x}_{b,xy}^{ ext{cmd}}$	2	m	-

Table S1: Position tracking observations

#### **A.2.2** Motion analysis metrics

The feet air time metric, shown in Fig. 7, is calculated as the total duration the feet remain off the ground, expressed as:

$$\sum_{j=1}^{n_{\text{feet}}} (t_{\text{air},j} - 0.5) \cdot \mathbf{1}_{\text{new-contact},j}$$

Table S2: Velocity tracking observations

Term	Notation	Dimension ANYmal   G1	Units	Noise
Observations				
Base linear velocity	$\mathbf{v}_t$	3	m/s	[-0.10, 0.10]
Base angular velocity	$oldsymbol{\omega}_t$	3	rad/s	[-0.20, 0.20]
Projected gravity	$\mathbf{g}_t^{ ext{proj}}$	3	-	[-0.05, 0.05]
Joint position	$\mathbf{q}_t$	12   37	rad	[-0.01, 0.01]
Joint velocity	$\mathbf{\dot{q}}_t$	12   37	rad/s	[-1.50, 1.50]
Previous action	$\mathbf{a}_{t-1}$	12   37	rad	-
Commands				
Linear x velocity	$v_x^{\mathrm{cmd}}$	1	m/s	_
Linear y velocity	$v^{\rm cmd}$	1	m/s	_
Angular yaw velocity	$\omega_z^{ m cmd}$	1	rad/s	-

Table S3: Position tracking reward terms (adapted from Rudin et al. [39])

Term	Equation	Weig	ght
	•	ANYmal	G1
Task			
Target position tracking	$(1 - 0.5 \cdot \ \mathbf{x}_{b,xy}^{\mathrm{cmd}}\ ^2) \cdot 1_{\{t > T - 3\}}$	10.0	10.0
Stability			
Linear z velocity	$v_z^2$	-2.0	-0.2
Angular roll-pitch velocity	$\ \omega_{xy}\ ^2$	None	-0.005
Flat orientation	$\ \mathbf{g}_{xy}^{ ext{proj}}\ ^2$	-1.0	-1.0
Joint limits	$\ \mathbf{q} - \mathrm{clip}(\mathbf{q}, \mathbf{q}_{\min}, \mathbf{q}_{\max})\ _1$	None	-1.0
Joint deviation (hip)	$\ \mathbf{q}_{hip} - \mathbf{q}_{default,hip}\ _1$	None	-0.1
Joint deviation (arms)	$\ \mathbf{q}_{arms} - \mathbf{q}_{default,arms}\ _1$	None	-0.1
Joint deviation (fingers)	$\ \mathbf{q}_{ ext{fingers}} - \mathbf{q}_{ ext{default,fingers}}\ _1$	None	-0.05
Joint deviation (torso)	$\ \mathbf{q}_{torso} - \mathbf{q}_{default,torso}\ _1$	None	-0.1
Applied torque limits	$\ oldsymbol{ au} - oldsymbol{ au}_{ ext{computed}}\ _1$	-0.2	-0.2
Joint velocity	$\ \dot{\mathbf{q}}\ ^2$	-0.001	-0.001
Joint velocity limits	$\ \dot{\dot{\mathbf{q}}}\  - \operatorname{clip}( \dot{\mathbf{q}} , 0.9 \cdot \dot{\mathbf{q}}_{\max})\ _1$	-1.0	-1.0
Contact forces	$\ \max\left(\ \mathbf{f}_{\text{contact}}\  - 700, 0\right)\ _1$	-1.0e-5	-1.0e-5
Collision	$\ \max\left(\frac{\ \mathbf{f}_{\text{contact}}\ }{200},1\right)\ _1$	-0.5	None
Feet slide	$\sum_{j=1}^{n_{\text{feet}}} \ \mathbf{v}_{\text{foot},j}\  \cdot 1_{\text{contact},j}$	None	-0.1
Smoothness			
Joint torques	$\  au\ ^2$	-1.0e-5	-2.0e-6
Joint accelerations	$\ oldsymbol{ au}\ ^2 \ oldsymbol{\ddot{q}}\ ^2$	None	-1.0e-7
Action rate	$\ \mathbf{a}_{t} - \mathbf{a}_{t-1}\ ^{2}$	-0.01	-0.005
Feet air time	$\ \mathbf{a}_{t} - \mathbf{a}_{t-1}\ ^{2}$ $\sum_{j=1}^{n_{\text{feet}}} (t_{\text{air},j} - t_{\text{thres}}) \cdot 1_{\text{new-contact},j}$	0.1	0.75
Base acceleration	$\ \dot{\mathbf{v}}_{\text{base}}\ ^2 + 0.02 \cdot \ \dot{\boldsymbol{\omega}}_{\text{base}}\ ^2$	-0.001	None
Feet acceleration	$\sum_{j=1}^{n_{ ext{feet}}} \ \dot{\mathbf{v}}_{ ext{foot},j}\ $	-0.002	None
Auxiliary			
Termination penalty	$1_{terminated}$	-200.0	-200.0
Stalling penalty	${f 1}_{\{\ {f x}_{b,xy}^{ m cmd}\ >0.25\}}\cdot{f 1}_{\{\ {f v}_{xy}\ <0.2\}}$	-1.0	-1.0
Exploration	$rac{\mathbf{v}_{xy}}{\ \mathbf{v}_{xy}\ } \cdot rac{\mathbf{x}_{b,xy}^{ ext{cmd}}}{\ \mathbf{x}_{b,xy}^{ ext{cmd}}\ }$	1.0	1.0
Stand still	$\ \mathbf{q} - \mathbf{q}_{\text{default}}\ ^2 \cdot 1_{\{\ \mathbf{x}_{b,xy}^{\text{cmd}}\  \le 0.1\}} \cdot 1_{\{t > T-1\}}$	-0.05	-0.05

Note:  $t_{\text{thres}} = 0.5$  for ANYmal and  $t_{\text{thres}} = 0.4$  for G1.

Table S4: Velocity tracking reward terms

Term	Equation	Weig	ght
	-	ANYmal	G1
Task			
Linear xy velocity	$\exp\left(-\ \mathbf{v}_{xy}-\mathbf{v}_{xy}^{\mathrm{cmd}}\ ^2/0.25\right)$	1.0	1.0
Angular yaw velocity	$\exp\left(-(\omega_z - \omega_z^{\text{end}})^2/0.25\right)$	0.5	1.0
Stability			
Linear z velocity	$v_z^2$	-2.0	-0.2
Angular roll-pitch velocity	$\ \omega_{xy}\ ^2$	-0.05	-0.05
Flat orientation	$\ \mathbf{g}_{xy}^{\text{proj}}\ ^2$	-5.0	-1.0
Undesired contacts	$1_{ ext{self-collision}}$	-1.0	None
Joint limits	$\ \mathbf{q} - \operatorname{clip}(\mathbf{q}, \mathbf{q}_{\min}, \mathbf{q}_{\max})\ _1$	None	-1.0
Joint deviation (hip)	$\ \mathbf{q}_{hip} - \mathbf{q}_{default,hip}\ _1$	None	-0.1
Joint deviation (arms)	$\ \mathbf{q}_{arms} - \mathbf{q}_{default,arms}\ _1$	None	-0.1
Joint deviation (fingers)	$\ \mathbf{q}_{ ext{fingers}} - \mathbf{q}_{ ext{default,fingers}}\ _1$	None	-0.05
Joint deviation (torso)	$\ \mathbf{q}_{torso} - \mathbf{q}_{default,torso}\ _1$	None	-0.1
Feet slide	$\sum_{j=1}^{n_{ ext{feet}}} \ \mathbf{v}_{ ext{foot},j}\  \cdot 1_{ ext{contact},j}$	None	-0.1
Smoothness			
Joint torques	$\ oldsymbol{ au}\ ^2 \ \ \ddot{f q}\ ^2$	-2.5e-5	-2.0e-6
Joint accelerations	$\ \ddot{\mathbf{q}}\ ^2$	-2.5e-7	-1.0e-7
Action rate	$\ \mathbf{a}_{t} - \mathbf{a}_{t-1}\ ^{2}$	-0.01	-0.005
Feet air time	$\sum_{j=1}^{n_{ ext{feet}}} (t_{ ext{air},j} - t_{ ext{thres}}) \cdot 1_{ ext{new-contact},j}$	0.5	0.75
Auxiliary			
Termination penalty	$1_{ ext{terminated}}$	None	-200.0

Note:  $\overline{t_{\text{thres}}} = 0.5$  for ANYmal and  $t_{\text{thres}} = 0.4$  for G1.

The contact frequency measures the total number of times the feet make contact with the ground and is given by:

$$\sum_{j=1}^{n_{\mathsf{feet}}} \mathbf{1}_{\mathsf{new-contact},j}$$

## A.2.3 Additional hardware experiments

In addition to the **Memory-Aug** policy, we also test the sim-to-real transfer of the **Baseline-Aug** policy, trained under the same terrain profiles. As shown in Figure S9, the robot exhibits limited adaptability when subjected to an ID joint failure, often losing balance and struggling to maintain stable locomotion while tracking the target. This behavior aligns with our simulation results, where the lack of context awareness in



Figure S9: Position tracking under ID (LF HAA) joint failure with **Baseline-Aug** policy.

the baseline policy limited its ability to identify and adapt to specific joint failures.

Table S5: Position tracking training details

Hyperparameter	ANYmal	G1
PPO hyperparameters		
Parallel environments	4,096	4,096
Steps per environment	48	48
Epochs per update	5	5
Minibatches per epoch	4	4
Discount rate $(\gamma)$	0.99	0.99
GAE parameter	0.95	0.95
Value loss coefficient	1.0	1.0
Clipping parameter	0.20	0.20
Entropy coefficient	0.005	0.003
Maximum gradient norm	1.00	1.00
Initial learning rate	0.001	0.001
Target KL	0.01	0.01
Optimizer	Adam	Adam
Policy Network architectures		
Policy $(\pi)$ MLP hidden layers	128, 128, 128	256, 128, 128
Critic $(V^{\pi})$ MLP hidden layers	128, 128, 128	256, 128, 128
MLP activations	ELU	ELU
Memory Module		
RNN type	LSTM	LSTM
RNN hidden size	256	256
RNN hidden layer	1	1

Table S6: Velocity tracking training details

PPO hyperparametersParallel environments $4,096$ $4,096$ Steps per environment $24$ $24$ Epochs per update $5$ $5$ Minibatches per epoch $4$ $4$ Discount rate $(\gamma)$ $0.99$ $0.99$ GAE parameter $0.95$ $0.95$ Value loss coefficient $1.0$ $1.0$ Clipping parameter $0.20$ $0.20$ Entropy coefficient $0.005$ $0.008$ Maximum gradient norm $1.00$ $1.00$ Initial learning rate $0.001$ $0.001$
Steps per environment         24         24           Epochs per update         5         5           Minibatches per epoch         4         4           Discount rate $(\gamma)$ 0.99         0.99           GAE parameter         0.95         0.95           Value loss coefficient         1.0         1.0           Clipping parameter         0.20         0.20           Entropy coefficient         0.005         0.008           Maximum gradient norm         1.00         1.00           Initial learning rate         0.001         0.001
Epochs per update         5         5           Minibatches per epoch         4         4           Discount rate $(\gamma)$ 0.99         0.99           GAE parameter         0.95         0.95           Value loss coefficient         1.0         1.0           Clipping parameter         0.20         0.20           Entropy coefficient         0.005         0.008           Maximum gradient norm         1.00         1.00           Initial learning rate         0.001         0.001
Minibatches per epoch44Discount rate $(\gamma)$ 0.990.99GAE parameter0.950.95Value loss coefficient1.01.0Clipping parameter0.200.20Entropy coefficient0.0050.008Maximum gradient norm1.001.00Initial learning rate0.0010.001
Discount rate $(\gamma)$ 0.99         0.99           GAE parameter         0.95         0.95           Value loss coefficient         1.0         1.0           Clipping parameter         0.20         0.20           Entropy coefficient         0.005         0.008           Maximum gradient norm         1.00         1.00           Initial learning rate         0.001         0.001
GAE parameter       0.95       0.95         Value loss coefficient       1.0       1.0         Clipping parameter       0.20       0.20         Entropy coefficient       0.005       0.008         Maximum gradient norm       1.00       1.00         Initial learning rate       0.001       0.001
Value loss coefficient1.01.0Clipping parameter0.200.20Entropy coefficient0.0050.008Maximum gradient norm1.001.00Initial learning rate0.0010.001
Clipping parameter         0.20         0.20           Entropy coefficient         0.005         0.008           Maximum gradient norm         1.00         1.00           Initial learning rate         0.001         0.001
Entropy coefficient0.0050.008Maximum gradient norm1.001.00Initial learning rate0.0010.001
Entropy coefficient0.0050.008Maximum gradient norm1.001.00Initial learning rate0.0010.001
Initial learning rate 0.001 0.001
•
TD 177
Target KL 0.01 0.01
Optimizer Adam Adam
Policy Network architectures
Policy $(\pi)$ MLP hidden layers 128, 128, 128 256, 128, 128
Critic $(V^{\pi})$ MLP hidden layers 128, 128, 128 256, 128, 128
MLP activations ELU ELU
Memory Module
RNN type LSTM LSTM
RNN hidden size 256 512
RNN hidden layer 1 1